Transaction B: Mechanical Engineering
Vol. 16, No. 4, pp. 344–353

SCIENTIA IRANICA

Experimental Analysis of Cavitaion Effects on Drag Force and Back Pressure of Circular Cylinder with Free Turbulence

I. Jafari Gavzan[1] **and M. Rad**[1]

Abstract. *The characteristics of a cavitation water tunnel test setup and the experiments of cavitation around a circular cylinder with free stream turbulence are presented in this paper. The Reynolds number of flow is limited in the range of 1.26×10^5 to 3×10^5 and the far upstream flow has free turbulence. Drag force, back pressure, location of cavitation inception, length of cavity and appearance of cavitation are measured or observed and their results are presented here. It was found that the cavitation effects on the boundary layer and separation of flow over the cylinder and drag force become minimum at the cavitation number of 1.94. The cavitation inception occurs in the sub-layer and at an angle of about 105°, with respect to flow direction (inception location depends on Reynolds number). The back pressure coefficient becomes maximum at the cavitation number of 1.94.*

Keywords: *Drag force; Cavitation tunnel; Free turbulence.*

INTRODUCTION

Cavitation is the rupture of a liquid caused by a reduction of local pressure. The rupture is induced by the formation of vapor bubbles. As the fluid moves into a region of high pressure, the bubbles will suddenly condense, in other words, collapse. After the bursting of the bubbles, very high jet velocities are produced, leading to local pressures of more than 500 atmospheres and local temperatures of over 2000°C during a time scale of less than a microsecond. The collapse of many bubbles may cause pitting at solid surfaces and high frequency sounds are generated. Cavitation can also be used in beneficial ways such as ultrasonic cleaners and cutters. Moreover, a sheet of bubbles or supercavitation can be used to reduce the drag of moving objects in liquids [1]. Some experiments have been performed about the location of cavitation inception and the associated cavitation number in the past [1,2]. However, the physics of cavitation phenomena, the correct location of cavitation inception and the effects of roughness and free turbulence on inception have not been truly understood. Only recently has the investigation on drag force, back pressure, actual thickness, length of cavity, different regions and type of cavitation on downstream and upstream flows been commenced in a systematic way. In addition, the nature of instabilities, investigation of induced frequencies, the mechanism and role of re-entrant jet, the real nature of bubble shedding, cloud cavitation, the mechanism of bubble collapse and several important subjects have not been elucidated completely. Knapp et al. [3] have performed several experiments on many different bodies. When the upstream boundary layer of a cylinder is laminar, cavitation initiates in the wake. Arakeri [4] has performed several experiments about the viscous effects on the inception location for a smooth sphere. He concluded that at the upstream of the cavitation area on the sphere, a boundary layer separation occurs. William et al. [5] investigated the location of cavitation inception and the noise due to the collapse mechanism of bubbles. They have conducted their experiment on laminar and turbulent boundary layer regions of a hydrofoil. Amromin [6], in an analytical and experimental investigation, concluded that the viscous effects on the inception location are not negligible for bubble and sheet cavitation. Of-

1. *Department of Mechanical Engineering, Sharif University of Technology, Tehran, Iran.*
*. *Corresponding author. E-mail:jafarigavzan@mech.sharif.edu*

Received 22 April 2008; accepted 4 October 2008

ten, a vortex cavitation is generated downstream of the sheet cavity, and such a vortex cavitation under the certain conditions generates a cloud cavitation. The investigation of vortex cavitation is possible if the circulation of the vortex and its core radius are known. Keller [7] in his investigation of scale effects, performed some experiments with different models and sizes of bodies. The cavitation theory assumes that the cavitation phenomena at the model and the prototype for geometrically similar bodies are identical at equal cavitation number values. But, experiment shows that there are differences in cavitation phenomena between the model and prototype at equal cavitation numbers. The most important scales are: size of model, upstream flow velocity and free turbulence. Sato et al. [8] measured the bubble nuclei populations in the wake of a circular cylinder under cavitating and non- cavitating conditions. In addition, the mean velocity defect and the turbulent fluctuations were monitored in order to try to understand the nuclei population dynamics within the flow. Batchelor [9] explains the inception and development of cavitation and the collapse of bubbles physically. Saito and Sato [10] carried out some experimental work on a shedding type of vortex cavity in the wake of a circular cylinder. This is a fundamental flow field in which the vortex cavitation with high impact appears. They observed that the cavities are shed periodically. This shedding-type cavity is divided into some parts and these are collapsed near the solid wall. Tsu et al. [11] have derived correction rules and conversion of a drag coefficient measured experimentally in a closed tunnel. The corresponding unbounded flow condition requires only the data of the conventional cavitation number and the tunnel-spacing ratio. Savchenko [12] provides a brief review of some investigations and new research into hydrodynamic supercavitation. Fabula [13] derived a linearized theory for a two-dimensional hydrofoil in a chocked-tunnel flow. Wang and Tsu [14] have shown that the unsteady disturbance generates a surface wave, which propagates downstream along the free cavity boundary. Dular and Bachert [15] proved that there is not a good agreement between experimental and numerical methods at the inception and development phase. Roshko [16] observed that if the boundary layer of the cylinder is turbulent, a laminar separation occurs at about 105. Korkuk and Atlar [17] installed screens before the test section for the propeller test. Brewer and Kinnas [18] measured and investigated the dimensions of a partial cavity on the hydrofoil. The mathematical solution was found with high approximation for supercavitation [19].

In this paper, the test method for the case of a circular cylinder, using the high speed cavitation tunnel at Sharif University of Technology, is presented and, then, the effects of cavitation on drag force, back pressure, angle of inception point and length of cavity are given. The type and conditions of cavitation are discussed in detail. The flow regimes vary from non-cavitating flow to inception, to a chocking condition.

CAVITATION TUNNEL CHARACTERISTICS

In contrast to a wind tunnel, high speed cavitation water tunnel design methods are not available in the literature. In a high speed cavitation tunnel design, if there is a small leakage of air, it prevents the formation of cavitation. The initial air and the released gas after cavitation inception are drained at several locations of the tunnel. The internal pressure at these locations is more than atmospheric pressure. In the construction of the Sharif tunnel, seven diffusers with divergent angles ranging from 3°to 10°and different lengths were used. The mentioned tunnel is shown in Figures 1 and 2. The four sides of the test section are provided with clear plexiglass windows for photographic and observational purposes. The test section and settling chamber are connected to each other with a high contraction ratio nozzle. The basic information of flow characteristics and working section sizes of the mentioned tunnel are explained as follows:

Maximum velocity in test section:	25 m/s
Maximum pressure of tunnel:	5 atm
Test section:	84 cm ×15 cm ×10 cm
Contraction ratio of nozzle:	17.3

EXPERIMENTAL EQUIPMENT AND INSTRUMENTS

1. Vacuum pressure gauge containing glycerin (calibrated), measuring the average back pressure;

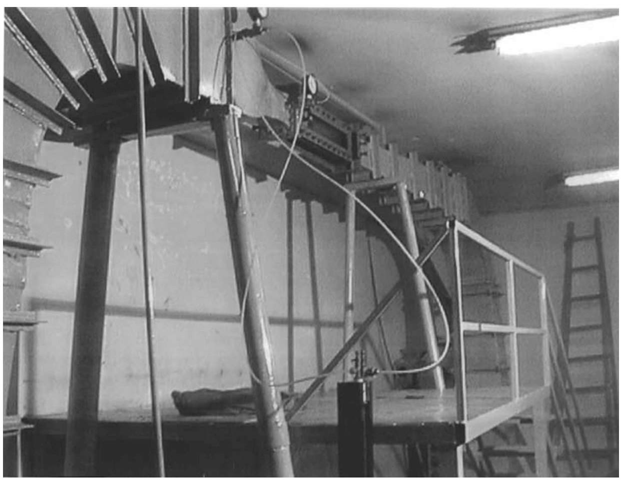

Figure 1. Sharif University high speed cavitation tunnel.

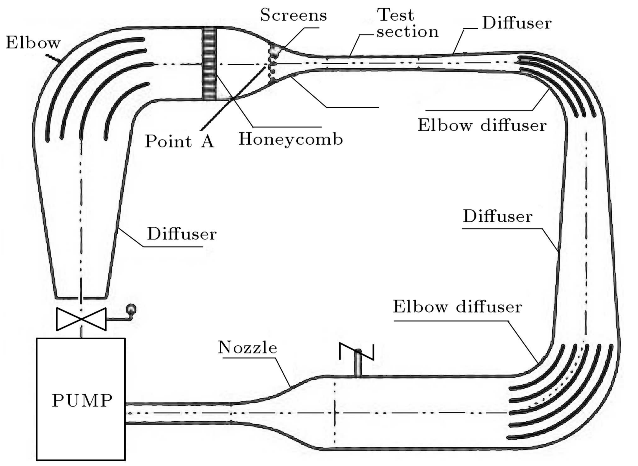

Figure 2. Schematic presentation of Sharif University high speed cavitation tunnel.

2. Vacuum pressure gauge without glycerin (calibrated) which presents the frequency and amplitude of the fluctuation;
3. Manometer (calibrated);
4. Pressure gauge (0-5 atm) (calibrated);

   4-1 Pressure gauge (0-2 atm) (calibrated).
5. Dynamometer measuring the drag force (of order 0-200 Newtons) (calibrated);
6. High speed camera (3000 frames/sec);
7. General equipment for measuring angles and dimensions.

THE TEST MODEL

A smooth black stainless steel circular cylinder with a diameter of 1.6 cm and length of 10 cm has been used as the model. For measuring the back pressure on the cylinder, two holes have been provided. The first is in the axial direction and has a length of 5.5 cm. The second hole is in the radial direction and the two holes are connected to each other (Figure 3). The diameter of the radial hole is very small. A three-way joint is installed to the axial hole. At the axial measuring hole, two pressure gauges are connected such that one of them is a vacuum gauge. Also, a valve for opening and closing the circuit of each pressure gauge is installed. At the beginning of the test, if the back pressure is higher than the atmosphere, the pressure gauge (0-2 atm) becomes open, otherwise the vacuum pressure gauge is utilized. A manometer, which connects the inlet and outlet of the nozzle, measures the pressure difference. The upstream flow and angle, θ, with respect to flow direction, are defined in Figure 4.

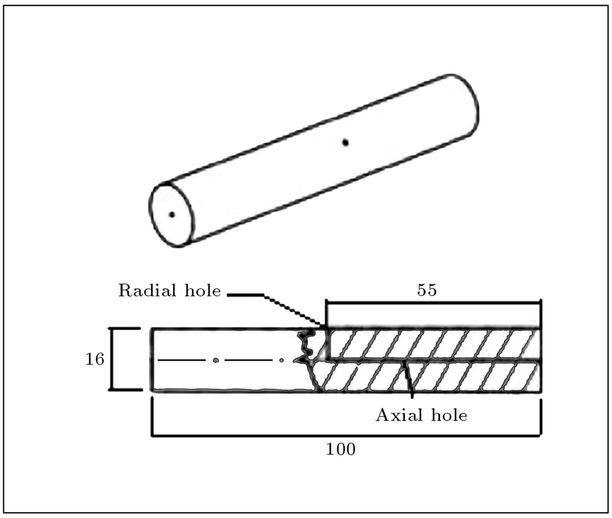

Figure 3. Model of circular cylinder with axial and radial holes.

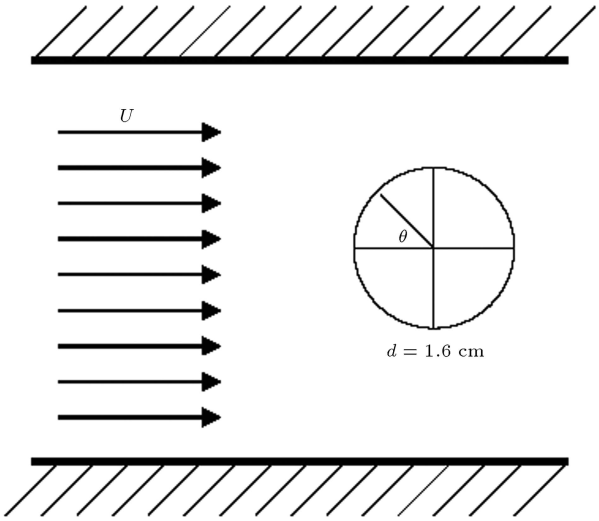

Figure 4. Circular cylinder section and upstream flow.

DRAG FORCE AND BACK PRESSURE MEASUREMENTS

It is common practice to quote the data of the drag and back pressure of the cylinder in the form of values of the drag and back pressure coefficients as defined below:

$$c_d = \frac{2D}{\rho U^2 A}, \qquad cp_b = \frac{P_b - P_\infty}{\frac{1}{2}\rho U^2}. \tag{1}$$

The measured values of velocity (U) and drag coefficient (c_d) in non-cavitating flow are corrected to obtain the corresponding values for an unbounded condition. D is the net drag force on the cylinder, U is the flow velocity at the nozzle exit and A is the area of the projection of the circular cylinder on a plane, normal to the stream at the nozzle exit. In the case of a two-dimensional cylinder, $A = bd$. Before measuring the drag force and back pressure, all equipment has been calibrated accurately. The drag and back pressure coefficients of the circular cylinder are functions of Reynolds number and turbulence intensity [9]:

$$c_d = f(\mathrm{Re},\ Tu), \tag{2}$$

$$cp_b = g(\mathrm{Re},\ Tu). \tag{3}$$

The drag of the model is obtained as follows:

$$D_{\mathrm{model}} = D_{\mathrm{total}} - D_{\mathrm{plate}}. \tag{4}$$

D_{plate} is the drag force of the flat plate when the model is installed at the test section.

For obtaining the value of the last term of the right hand side, the model is connected to the opposite wall such that a very small gap exists between the cylinder and the plate at all corresponding cavitation numbers for every velocity. Figure 5 shows the drag force of the flat plate when the testing model is removed from the test section. The drag force of the flat plate, which is attached to the dynamometer after cavitation inception, is a function of model diameter, upstream flow velocity and cavitation number:

$$D_{\mathrm{plate}} = f(d, U, \sigma). \tag{5}$$

When U and d become constant, the above relation may be written as follows:

$$D_{\mathrm{plate}} = g(d, U).h(\sigma). \tag{6}$$

The experiment shows that $h(\sigma)$ is a decreasing function of σ. Figure 6 gives the D_{plate} as a function of σ at $U = 9.5$ m/s. This process is repeated for all velocities (8.2 m/s $\leq U \leq$ 18.7 m/s).

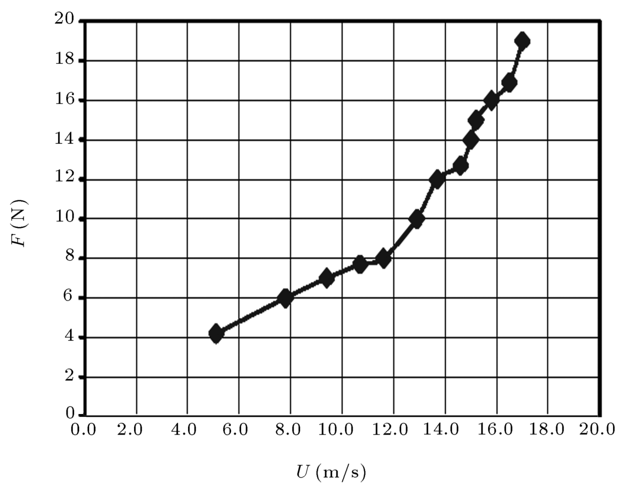

Figure 5. Drag force of the flat plate with respect to the velocity.

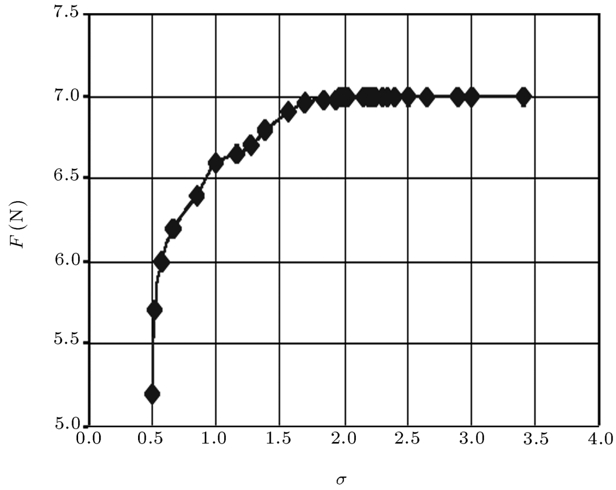

Figure 6. Drag force of the flat plate due to interaction with respect to cavitation number ($U = 9.5$ m/s).

In the Sharif University high speed cavitation tunnel, for the laminar experiment, a conventional honeycomb at the exit of the settling chamber is installed. But, for a turbulent experiment, several screens, in series, are installed in the nozzle just before its inflection point (point A, Figure 2) to generate free turbulence. The turbulence intensity at the exit of the nozzle depends on its wall contour, the location and size of screens and the contraction ratio in this experiment. At the range of Reynolds number of 1.26×10^5 to 3×10^5, the upstream flow has free turbulence verified by the measured back pressure and drag force of the model (see the next section).

VALIDATION OF EXISTENCE OF FREE TURBULENCE IN UPSTREAM FLOW

Free turbulence in the far upstream flow causes the boundary layer on the forward side of the cylinder to become turbulent. Then, a marked increase in the approximately uniform pressure in the broad wake region at the back of the cylinder occurs. The measurement of drag force for the mentioned cylinder shows a large decrease at a range of Reynolds numbers of 1.26×10^5 to 3×10^5. Thus, when the transition to turbulent flow in the boundary layer occurs, the position of separation of the boundary layer moves back, verified by the measured back pressure and its distribution on the circular cylinder in the non-cavitating flow (Figure 7, A to B).

The experiment shows that, in non-cavitating flow at the Reynolds number of 1.5×10^5 and cavitation number of 3.41, the drag coefficient of the cylinder is 0.51. When $2.21 < \sigma \leq 3.41$, c_d has a constant value of 0.51 (Figure 8, A to B). The back and surface pressure are measured and the measurement shows that the back

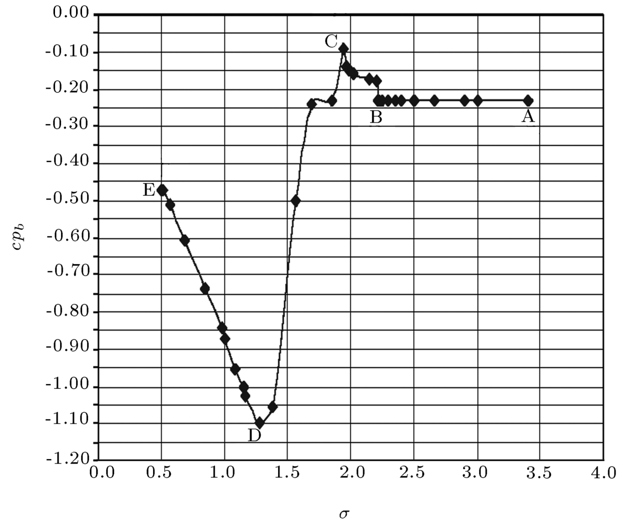

Figure 7. Back pressure coefficient of the circular cylinder with respect to cavitation number.

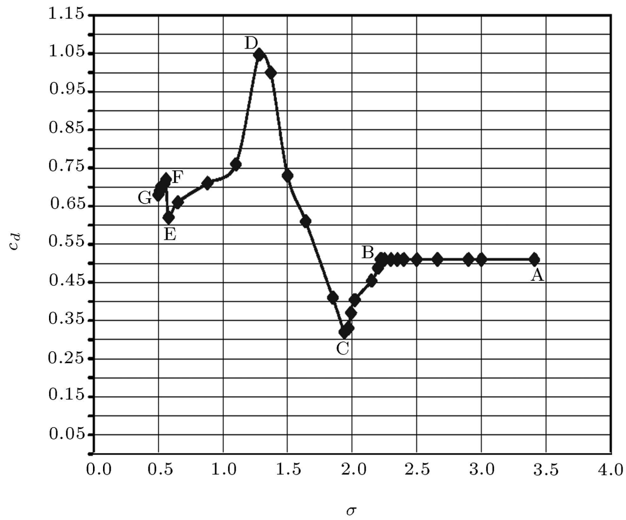

Figure 8. Drag force coefficient of the circular cylinder with respect to cavitation number.

pressure is very high in non-cavitating flow, as follows:

$$cp_b = -0.231, \qquad \sigma > 2.21.$$

Since at the range of Reynolds numbers of 1.26×10^5 to 3×10^5 the back pressure and drag force coefficients are -0.231 and 0.51, respectively, the boundary layer of the cylinder is in a transition phase or turbulent. In non-cavitating flow, for specifying the effects of free turbulence at the higher Reynolds numbers, e.g. 2×10^5, the velocity of the upstream flow and the tunnel pressure are increased simultaneously. Then, the back pressure and drag force are measured. This process is performed at several Reynolds numbers and, at each step of the experiment, the tunnel pressure should be increased.

CAVITATION INCEPTION

A cavitation inception test was carried out for a model of the circular cylinder. In this test, the effect of cavitation on the drag force and back pressure near the inception is studied. The flow in the upstream of the model is in the range of Reynolds numbers of 1.26×10^5 to 3.2×10^5, which has free turbulence.

The following procedure of inception measurements is performed. The tunnel flow velocity (U) is kept constant (of course during each test case). The static pressure is reduced slightly and then the drag force and back pressure are measured at each flow velocity. Measurements show that at the cavitation number of (2.20), the drag force decreases and the back pressure coefficient increases so that c_d becomes 0.488 and $cp_b = -0.19$ (Figures 7 and 8, just after B). In other words, when the cavitation number approaches (2.20), sensible changes in the back pressure and drag force coefficients occur.

Because the cavitation number depends on the tunnel static pressure, by lowering the tunnel static pressure, the cavitation becomes observable very close to the surface of the model at the angle of about 105°(inception location depends on Reynolds number). In this condition, the determined cavitation number, the measured drag force and back pressure coefficients are equal to 2.02, 0.404 and -0.16, respectively.

During the decrease of the cavitation number, by lowering the tunnel pressure little by little, the Reynolds number and turbulence intensity does not vary. Therefore, on the basis of Relations 2 and 3, the drag force and back pressure coefficients should not vary, but they change very close to σ of 2.20, considerably, and also at σ of 2.15, we have $c_d = 0.454$ and $cp_b = -0.175$. So, the inception cavitation number is approximately equal to 2.20. At $\sigma \leq 2.20$, the drag and back pressure coefficients are functions of the following dimensionless parameters:

$$c_d = f(\mathrm{Re}, Tu, \sigma), \tag{7}$$

$$cp_b = g(\mathrm{Re}, Tu, \sigma). \tag{8}$$

For specifying the inception cavitation number and the location of cavitation at the higher Reynolds number, the velocity of upstream flow is increased to obtain the desired Reynolds number. Then, the tunnel pressure is increased slowly until the non-cavitating flow condition occurs. In this step, the tunnel pressure and the velocity of upstream flow are recorded. Then, for initiating cavitation, the tunnel pressure is lowered.

At the cavitation number of 2.20, cavitation occurs but is not observable and its location in the flow field around the body is not known (probably at $\theta = 105°$). The back pressure coefficient of the cylinder increases considerably. When σ is equal to 2.15, $c_d =$

0.42, so cavitation exists but is not observable. From inception until sheet cavitation, the second separation point moves towards the back as follows:

$$\theta s(2.20) < \theta s(2.15) < \theta s(2.02) < \theta s(1.94).$$

By measuring the surface pressure of the cylinder at each cavitation number, the limit of nearly uniform pressure at the back of the model is specified.

CAVITATION AND ITS EFFECTS AFTER INCEPTION

Several points during the conduction of the experiment which are very sensitive important are mentioned below:

1. Inception cavitation number;
2. Inception location;
3. The cavitation effect on drag force from inception to super cavitation regimes;
4. The cavitation effect on back pressure and the length of cavity.

In order to know the effects of cavitation on the drag force and back pressure of the cylinder, many experiments have been carried out in the high speed cavitation tunnel. Experiments have been performed at different pressures and velocities. At the moment of cavitation inception, no change in the fluctuating characteristics of the back pressure (frequency and amplitude) occurs, but the back pressure coefficient increases from -0.231 to -0.18.

As the value of σ is reduced, the value of cp_b increases very slightly and cavitation occurs at the σ of 2.2 (Figure 7). At $\sigma \approx 2.02$, cavitation becomes observable very close to the surface of the cylinder at about $\theta \approx 105°$. cp_b increases from -0.175 to -0.16 and the drag force coefficient also decreases, its value becoming 0.404. When $\sigma < 2.20$, c_d will depend on σ strongly (Figure 8, B to G).

$$\text{At } \sigma = 1.99: \quad cp_b = -0.14, \qquad c_d = 0.37,$$

and:

$$\text{at } \sigma = 1.97: \quad cp_b = -0.13, \qquad c_d = 0.33.$$

An important state occurs at σ of 1.94; where the drag coefficient reaches a global minimum value and the back pressure coefficient becomes absolute maximum. The values are as follows:

$$c_d = (c_d)_{\min} = +\,0.32, \qquad cp_b = (cp_b)_{\max} = -0.09.$$

If the boundary layer of the cylinder becomes laminar, such a relation between the back pressure and drag force coefficients does not exist.

Also, a thin sheet of cavity attached to the surface of the model is established from $\theta = 95°$ to $\theta = 110°$ approximately. Figure 9 gives the cavity length as a function of σ. The angle of the cavity leading edge is shown in Figure 10. If the cavitation number becomes less than 1.94, the trailing edge of the cavity grows fast toward downstream and the drag force increases. The back pressure fluctuates with high frequency and small amplitude at σ of 1.85. As the value of σ is reduced (taking the value of 1.64), the back pressure fluctuates with high frequency and large amplitude. For this condition, we may have $cp_b = -0.24$ and $c_d = 0.61$.

$$\text{At } \sigma = 1.5: \quad cp_b = -0.5, \qquad c_d = 0.73,$$

$$-\,0.696 \leq cp_b \leq -0.298.$$

There is a vortex shedding at the back of the model (Figure 11a). The life of a vortex cavity may be very

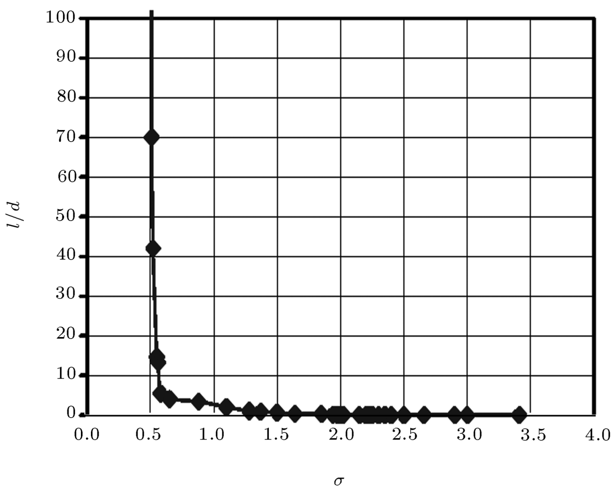

Figure 9. Cavity length with respect to cavitation number.

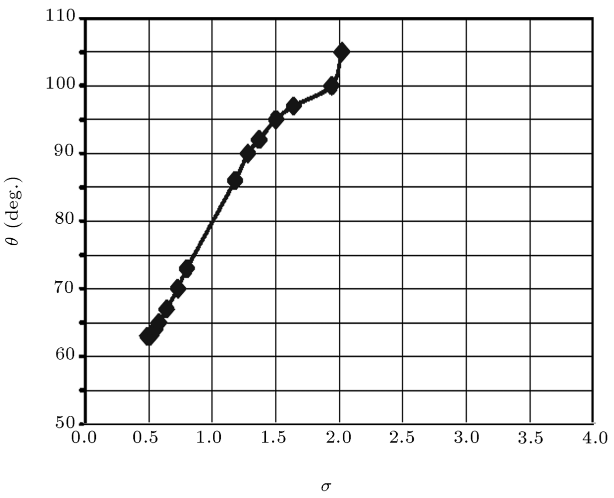

Figure 10. Angle of cavity inception with respect to σ.

(a)

(b)

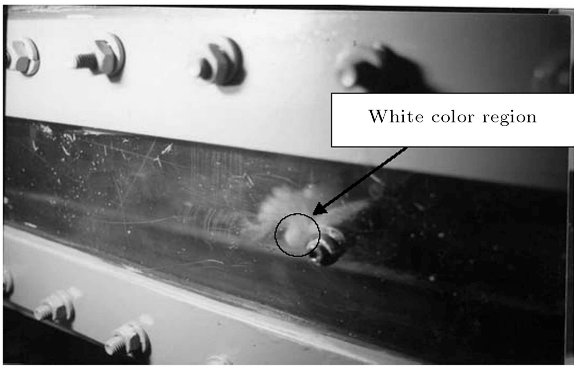

(c)

Figure 11. a) Shedding at the back of cylinder; b) Motion of vortex and its collapse rate (from a qualitative point of view); c) White color region at the back of model ($\sigma = 1.28$).

long and the rate of its collapse slow, since the liquid of the vortex has considerable angular momentum. Figure 11b shows that the collapse occurs during the motion of the vortex.

At $\sigma = 1.37 : cp_b = -1.056$, $c_d = 1.00$ and the leading edge of the cavity is very close to $\theta = 90°$.

Decreasing σ to 1.28, the measurements show that cp_b is a global minimum and c_d is a global maximum. Also, the leading edge of the cavity coincides with $\theta = 90°$.

Therefore, at $\sigma = 1.28 : cp_b = (cp_b)_{\min} = -1.097$, $c_d = (c_d)_{\max} = 1.047$.

At the cavitation number of (1.28), the drag force is maximum and the length of the white color area at the back of the cylinder is approximately equal to the diameter of the model. Also, there is vortex shedding at the trailing edge of the cavity (Figure 11c). The back pressure fluctuation has a small amplitude and low frequency.

A small reduction in the cavitation number causes a small increase in cp_b and a considerable decrease in c_d, i.e. at $\sigma = 1.17 : cp_b = -1.027$, $c_d = 0.80$; the angle of the cavity leading edge is approximately equal to 86°. The length of the white color area fluctuates between $2d$ and $1.7d$ at the back of the model and its frequency is also high. After a cavitation number of 1.17, the length of cavity increases fast, so it becomes very sensitive to the changes of σ. From $cp_b = -1.027$ to -0.73, the back pressure does not vary practically and $p_b = 22.1$ KN/m^2 because an observable transparent condition has appeared at the back of the model at this step.

A decrease in the drag coefficient in the range of $-1.027 \leq cp_b \leq -0.73$ is established only by the forward slow motion of the leading edge of the cavity region and the upstream pressure drop. Figure 12 shows two different lengths and appearances of cavitation at the same cavitation number. Therefore, as the back pressure coefficient becomes minimum, the value of the back pressure remains constant until the second relative minimum drag coefficient occurs.

When the second minimum drag coefficient occurs, the back pressure coefficient will be -0.512. Also, a mirror transparent (vacuum) appearance begins at $\theta = 180°$ and, after that, the back pressure becomes constant practically. The back pressure limit will be 13.6 KN/m^2. The change of non-dimensional cavity length, with respect to σ, as the transparent appearance becomes observable, will be absolutely large. At $\sigma = 0.58 : cp_b = -0.512$, $c_d = c_{d(\min)} = 0.64$ and the angle of the cavity leading edge with respect to the stagnation point is about 65°.

At the cavitation number of 0.56, a transparent and glassy appearance (vacuum) at the back of the model establishes; it has a length of $6.7d$ and, also, its leading edge begins at $\theta = 90°$. When σ is reduced slightly, the drag force decreases again due to the small progress of the leading edge of the attached bubble. As the transparent appearance commences, the drag force of the model increases smoothly until the leading edge of the pure vapor reaches the close top point and then c_d decreases. When supercavitation occurs (Figure 13), the measurements show that, at $\sigma \approx 0.49$, we have:

$$cp_b = -0.472, \qquad c_d = 0.68, \qquad \theta = 63°,$$

$$-d(l/d)/d\sigma \approx \infty.$$

(a)

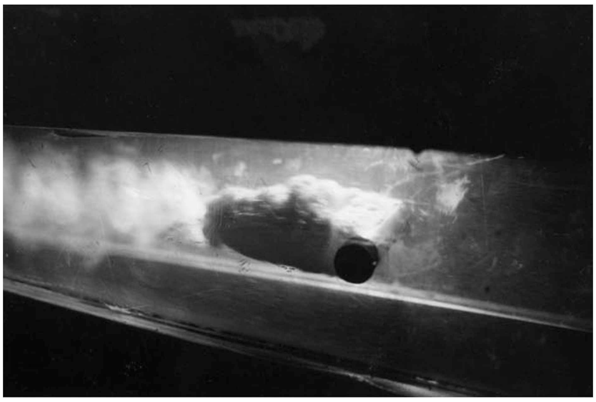

(b)

Figure 12. The cavitation number is the same for (a) and (b) at two different times.

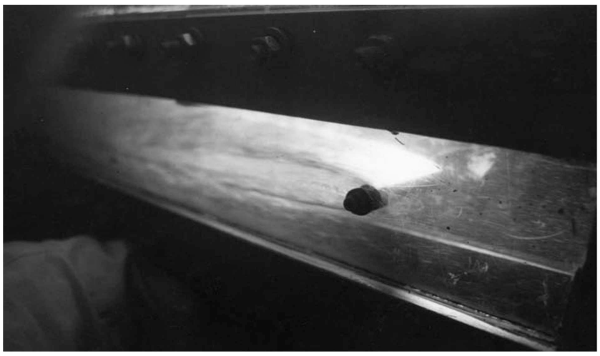

(a)

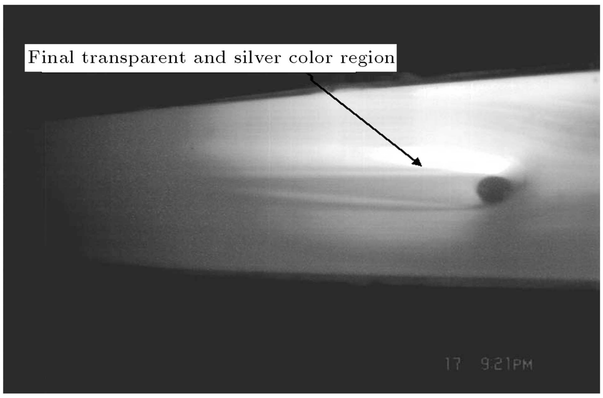

(b)

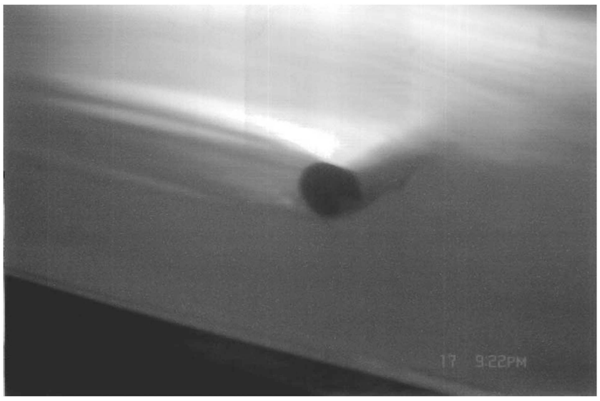

(c)

Figure 13. Supercavitation. a) There is only lateral vibration of the attached cavity bubble; b) The leading edge of supercavity has negligible oscillation; c) In this condition chocking has occurred ($\sigma \approx 0.49$).

CONCLUSION

The experiment shows that just after cavitation inception, from $\sigma = 2.20$ to $\sigma = 1.94$, the wake pressure coefficient gradually increases. In this phase, the phenomena of cavitation causes the second separation point to delay. The pressure coefficient in the sub-layer separation region, before initiating cavitation, becomes approximately -2.20 and its location is limited in $100° \leq \theta \leq 110°$. When reducing the cavitation number after inception, at $\sigma = 2.02$, the cavitation is observable momentarily at about $\theta = 105°$. It appears and disappears frequently at $\sigma = 1.99$ around $\theta = 105°$. The drag force decreases from $\sigma = 2.20$ to $\sigma = 1.94$ smoothly. The cavitation occurs in the laminar sub-layer (the first separation region at the back of the cylinder). Therefore, the turbulent separation point (second separation) is transferred more to the back of the cylinder. As a thin cavity layer (sheet cavity) attached to the model is formed, from $\theta = 95°$ to $\theta = 110°$, the drag force becomes minimum and its coefficient has a value of 0.32 at $\sigma = 1.94$. After this condition, the trailing edge of the thin cavity fluctuates with high frequency. The back pressure coefficient decreases and the drag force acting on the model increases fast.

At $\sigma = 1.28$, the drag force coefficient has an absolute maximum value of 1.047 due to two reasons:

1. The back pressure coefficient reaches to an absolute minimum value of -1.097;
2. The leading edge of the white color cavity region at the back of the model coincides with $\theta = 90°$.

Just before beginning the glassy and transparent condition at the back of the cylinder, the drag coefficient reaches a relative minimum value of 0.62 or 0.65. Then, c_d increases gradually until its value is equal to 0.72. In this condition, a single large cavity bubble at the net vapor phase establishes from $\theta = 90°$ to far downstream of the model. Then, the drag force coefficient decreases with a small rate and ends up at a limited value of 0.68. Drag reduction in this process is due to moving back forward the leading edge. The final θ, associated to the super cavitation state for the turbulent boundary layer at the forward side of the model, approaches 63°.

An important result about the fluctuation behavior of the back pressure is as follows: There is a white color region behind the cylinder; the wake flow is a mixture of vapor and water, that is, collapse occurs in generating the vapor area; there are always abrupt pressure changes, but as soon as the glassy and transparent condition appears, fluctuation becomes negligible (there is only the vapor phase); and the cavitation number corresponding to the inception of the glassy and transparent condition is (0.7). As the above state occurs, the longitudinal fluctuation of the attached cavity bubble becomes low, but lateral oscillation is noticeable (the buoyancy force in this case is very important). When the forward side boundary layer of the circular cylinder is laminar, the absolute minimum back pressure coefficient will be -2.45, but its value in the transition phase to the turbulent case is equal to (-1.097).

NOMENCLATURE

b	length of circular cylinder
c_d	drag force coefficient
cp_b	back pressure coefficient
d	diameter of circular cylinder
D_{total}	total measured drag force
F	the drag force of flat plate (Newton)
l	length of cavity
P_b	back pressure
p_v	vapor pressure of water
p_∞	static pressure at free stream
Re	Reynolds number Ud/ν
Tu	turbulence intensity
U	velocity at nozzle exit
$-d(l/d)/d\sigma$	the change of non-dimensional cavity length with respect to σ

Greek Symbols

ρ	water density
θ	angle with respect to upstream stagnation point
θs	separation angle
ν	kinematics viscosity of water
σ	cavitation number $(P\infty - Pv)/(\rho U^2/2)$

REFERENCES

1. Franc, J.P. and Michel, J.M., *Fundamentals of Cavitation*, Kluwer Academic Publisher, Dordrecht, London, UK (2004).
2. Rad, M. and Jafari Gavzan, I. "Test on Sharif University tunnel around hydrofoils and different shape models", *Research Proceeding*, SUT, D.M.E., Academic year (2005-2006).
3. Knapp, R.T, Daily, J.W. and Hammit, F.G., *Cavitation*, McGraw-Hill, New York, USA (1970).
4. Arakeri, V.H. "Viscous effects on the position of cavitation separation from smooth bodies", *JFM*, **68**, pp. 779-799 (1974).
5. William, K.B., Wolper, M.J. and Geib, F.E. "Cavitation noise and inception as influenced by boundary-layer development on a hydrofoil", *JFM*, **80**, part 4, pp. 617- 640 (1977).
6. Amromin, E. "Analysis of viscous effects on cavitation", *Appl. Mech.*, **53**(11), pp. 307-322 (Nov. 2000).
7. Keller, A.P. "Cavitation scale effects", *Fourth International Symposium on Cavitation (cav2001)*, California, (June 20-23 2001).
8. Sato, K., Liu, Z. and Brennen, C.E. "The microbubble distribution in the wake of a cavitating circular cylinder", *Cavitation and Multiphase Flow, ASME FED*, **153**, pp. 75-80 (1993).
9. Batchelor, G.B., *An Introduction to Fluid Dynamics*, Cambridge University Press, London, UK (1967).
10. Saito, Y.A. and Sato, K. "Cavitation bubble collapse and impact in the wake of circular cylinder", *Fifth International Symposium on Cavitation (cav2003)*, Osaka, Japan (November 1-4 2003).
11. Yao-Tsu, W.T., Brennen, C.E. and Whitney, A.K. "Cavity flow, wall effects and correction rules", *JFM*, **49**, part 2, pp. 223-256 (1971).
12. Savchenko, Y.N. "Super cavitation-problems and perspectives", *Fourth International Symposium on Cavitation (cav2001)*, California (June 20-23 2001).
13. Fabula, A.E. "Chocked flow about vented or cavitating hydrofoils", *Journal of Basic Engineering*, pp. 561-568 (Sept. 1964).
14. Wang, D.P. and Yao-Tsu, W.T "General formulation of a perturbation theory for unsteady cavity flows", *Journal of Basic Engineering*, pp. 1006-1100 (Dec. 1965).
15. Dular, M. and Bachert, R. "Experimental evaluation of numerical simulation of cavitating flow around hydrofoil", *European Journal of Mechanics B/Fluids*, **24**, pp. 522-538 (2005).

16. Roshko, A. "Experiments on the flow past a circular cylinder at very high Reynolds numbers", *JFM*, pp. 345-356 (1960).

17. Korkut, E. and Atlar, M. "On the importance of the effect of turbulence in cavitation inception tests of marine propellers", *Proc. R.SOC. Land*, pp. 29-48 (2002).

18. Brewer, W.H. and Kinnas, S.A. "Experiment and viscous flow analysis on a partially cavitating hydrofoil", *Journal of Ship Research*, **41**(3), pp. 161-171 (Sept. 1997).

19. Terentiev, A. "Mathematical modeling of cavitating flows", *Fifth International Symposium on Cavitation (cav2003)*, Osaka, Japan (November 1-4 2003).